Microporous and Mesoporous Materials 305 (2020) 110366

Contents lists available at ScienceDirect

Microporous and Mesoporous Materials

journal homepage: http://www.elsevier.com/locate/micromeso

Composite of Pt/AlSBA-15+zeolite catalyst for the hydroisomerization of n-hexadecane: The effect of platinum precursor

Monika Fedyna [a,*], Andrzej Żak [b], Karolina Jaroszewska [b], Jakub Mokrzycki [b], Janusz Trawczyński [b]

[a] Faculty of Chemistry Jagiellonian University, ul. Gronostajowa 2, 30-387, Kraków, Poland
[b] Wrocław University of Science and Technology, Wybrzeże Wyspiańskiego 27, 50-370, Wrocław, Poland

ARTICLE INFO

Keywords:
Hydroisomerization
Platinum precursors
Biporous materials
AlSBA-15
BEA zeolite
Composite materials

ABSTRACT

In this study, the Pt (0.5 wt%) catalysts supported on the bimodal composite materials consisting of AlSBA-15 and BEA zeolite, were prepared using three different precursors of Pt, *i.e.* H_2PtCl_6, $Pt(NH_3)_4(NO_3)_2$ and $Pt(NH_3)_4Cl_2$. The obtained catalysts were characterized by means of N_2 sorption, XRD, *Py*–FTIR, FTIR, H_2 chemisorption and TEM to determine the effect of the Pt precursor on their physicochemical properties. Catalytic performance of obtained catalysts was investigated in hydroisomerization of *n*-hexadecane. It was found, that the Pt precursor had significant impact on catalytic activity and selectivity. The results of *n*-hexadecane hydroconversion showed that the catalyst obtained with $Pt(NH_3)_4(NO_3)_2$ provided the highest yield of the most desired high-cetane number products. In addition, it had the lowest selectivity to cracking products, which are undesirable in hydroconversion of long-chain alkanes.

1. Introduction

Hydroisomerization of the *n*-alkanes is an important process in the production of high-quality fuels [1–3]. The branching of normal long chain alkanes enables the production of diesel fuel with improved cold flow properties [4] - the branched alkanes are characterized by lower temperature of cloud point and cold filter plugging in comparison with their normal analogues [5]. Thus, in recent years the process became more common. Additionally, the researchers aim to investigate new sources of long chain *n*-alkanes, thus its production from alternative energy carriers, especially from biomass resources is growing attention. Such fuels include the fractions obtained from *bio*-syngas in Fischer-Tropsch (FT) synthesis as well as those produced by hydroconversion of vegetable oils (HVO – Hydrotreatment of Vegetable Oils) [6]. The FT synthesis from *bio*-syngas technology is currently applied by Linde Engineering Dresden and HVO technologies lived to see the realization of industrial processes *inter alia* by Neste Oil (NExBTL license) [7] and Honeywell/UOP (Ecofining license) [8]. Typically hydroisomerization of *n*-alkanes takes place over the bifunctional catalysts containing both metal, which provides active sites for hydrocarbons dehydrogenation/hydrogenation and the Brønsted acid sites on which skeletal isomerization of carbocations occurs. According to classical mechanism of isomerization and cracking of alkanes, hydroconversion of alkanes involves few steps (Scheme 1) [9–11]. In the first step, *n*-alkanes are dehydrogenated on metal sites to olefins. Next, olefins diffuse into the Brønsted acid sites where they are subsequently protonated to form of the corresponding alkylcarbenium ions. The resulting carbenium ions undergo: (*i*) skeletal rearrangement *via* protonated cyclopropane (PCP) intermediates, (*ii*) alkyl shift and (*iii*) hydride shift or *β*-scission of C–C bond. Subsequently, these ions are deprotonated and hydrogenated over metal sites to form *i*-alkanes (mono- and multibranched isomers) and cracking products. In order to improve the performance of isomerization catalysts of long-chain alkanes, much attention is paid to ensure an adequate metal/acid balance, which strongly affects the properties of a catalyst, especially its selectivity towards isomerization [12,13] and consequently the yield of isomers. It can be found in many reports, that the adequate metal/acid balance can be controlled by several factors: (*i*) the preparation method of support and catalyst [14–16], (*ii*) the textural and chemical properties of support (concentration of acid sites and diffusion rate in the pores) [17,18], (*iii*) the nature of the metal precursor (dehydrogenation/hydrogenation activity and number of metal sites) [19–21] and (*iv*) the distance between the metal and Brønsted acid sites [22,23].

Dehydrogenation/hydrogenation properties of bifunctional catalysts

* Corresponding author.
E-mail address: monika.fedyna@uj.edu.pl (M. Fedyna).

https://doi.org/10.1016/j.micromeso.2020.110366
Received 16 March 2020; Received in revised form 29 April 2020; Accepted 28 May 2020
Available online 13 June 2020

are generally provided by the noble metals in mono- or bimetallic systems, usually Pt and Pd. The concentration of metal sites must be sufficient to: (*i*) supply a maximum amount of alkene intermediates to the acid sites, (*ii*) hydrogenate rapidly the primary branched carbenium ions and (*iii*) limit the scission of C–C bond. It was proved, that even small amounts of Pt (about 0.5 wt%) may provide sufficient activity of the catalyst (dehydrogenation/hydrogenation) to balance the acid sites [24]. Thus, a single metallic site with high activity (Pt or Pd) can balance several acid sites, depending on their strength [25]. It is also known that with the increase of the amount of metal content, the dispersion decreases and consequently the size of the metal particles increases as a result of agglomeration and sintering [19]. The uneven distribution of the metal particles and the presence of its agglomerates on the outer surface of the support, deteriorates the hydrogenation/dehydration properties of the metallic sites. As a result, a decrease in selectivity to isomers can be observed. Furthermore, carbon deposition on the surface of the catalyst occurs. In order to ensure high metal dispersion, high surface area of active phase and finally the activity of the catalyst, several methods of metal incorporation can be used. In the case of catalysts based on zeolites, as a method of metal distribution, ion exchange can be applied, where metal cations *i.e.* Pt or Pd exchange the cations *i.e.* H^+ or Na^+ present in zeolite [26]. For catalysts supported on SiO_2, Al_2O_3 and ordered mesoporous materials, the deposition of active phase is usually provided by impregnation method. For impregnation, various platinum salts can be used *i.e.* $Pt(NO_3)_2$ [19,27], H_2PtCl_6 [28–30], $Pt(NH_3)_4Cl_2$ [31], $Pt(NH_3)_4(NO_3)_2$ [4] and $Pt(NH_3)_4(OH)_2$ [32]. The type of metal precursor used for impregnation of the support, affects the location of the metal particles (*i.e.* on the outer or inner surface of the support) and the distance between the metallic and Brønsted acidic sites [14]. The distribution of metal sites also depends on the type of the support *i.e.* texture, distribution and strength of the acid sites [33]. Therefore, there are some discrepancies in the literature regarding the influence of platinum precursor differing with the valence state of Pt, its form (in cationic or anionic group), and the presence of chlorine or ammonium ions on size of metal particles and dispersion. The results of Belopukhov et al. [31] and Mäki-Arvela et al. [16,34] research revealed, that the use of $[Pt(NH_3)_4]^{2+}$ - based salts led to small Pt particles. As a result, the obtained Pt catalysts were characterized by higher metal dispersion and higher catalytic activity in comparison with catalyst obtained from H_2PtCl_6. The authors explained that the higher activity of catalysts prepared with $[Pt(NH_3)_4]^{2+}$ were a result of the high metal dispersion and small degree of intimate of the metallic and acidic sites. The use of the $[Pt(NH_3)_4]^{2+}$ precursors, allowed to locate the Pt near the acid centers and to reduce the distance between active centers. Meanwhile, the use of $[PtCl_6]^{2-}$ caused deposition of Pt on the supports surface and formation of a large Pt particles. Consequently, it led to increase of the distance between two active sites, thus the diffusion time of intermediates between metal and acid sites was extended and increased the probability of cracking. On the other hand Wang et al. [19] showed, that the catalysts prepared with use of an anionic precursors *i.e.* H_2PtCl_6 or $(NH_4)_2PtCl_4$, were characterized with better activity and higher yield of isomers, than those made using a cationic Pt precursors. The authors attributed better catalytic properties of the catalysts prepared with use of anionic precursors of Pt, to smaller particle sizes and higher Pt dispersion. Chandler et al. [35] revealed, that the presence of chlorine in the Pt precursor affected the size of the metal particles. For catalysts containing chlorine ions, a reduction of the crystal size of metal particles was observed and as a consequence the Pt dispersion increased. A similar effect was not observed for catalysts containing chlorine ions and amine groups in precursors of Pt, due to autoreduction of Pt species by NH_3 during calcination stage. Wang et al. [19] and Antoniassi et al. [36] proved, that the valence state of Pt in precursor (in the form of cation Pt (II) or anion containing Pt(IV)) affected crystallographic orientation of the particle facets on support surface. The catalysts prepared with use of H_2PtCl_6, exhibited smaller Pt particles in crystal orientation (1 1 1) which are more active in hydrogenation/dehydrogenation of hydrocarbons. Usage of the cationic precursor caused creation of larger Pt particles with the crystallographic orientation of the particle facets Pt (1 0 0). Despite the development that was made in the synthesis of catalysts for n-alkanes branching, the precise design of the catalyst composition to achieve the optimal activity, practicability and economic productivity still remains valid. To the best of the authors knowledge, no papers considering the impact of Pt precursor in the case of micro-mesoporous carriers were published. Most of the works regarding the impact of Pt precursor were referred to the single component supports *i.e.* Al_2O_3 [37], SiO_2 [38], SAPO-11 [39], SBA-15 [40], zeolites [19,39] and related materials (physical mixture of zeolite and ordered mesoporous material or zeolite and inert materials [41,42]) in powder form. Our investigation concerned the influence of platinum precursor on physicochemical properties and catalytic activity of Pt catalysts supported on

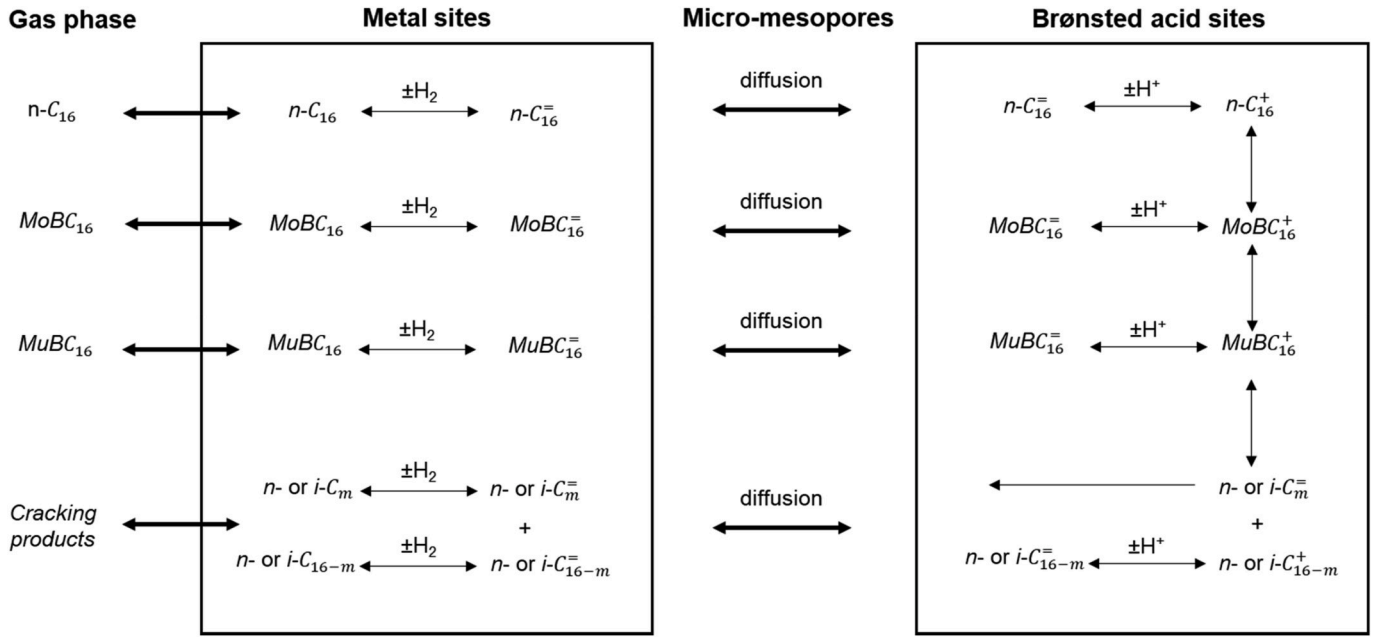

Scheme 1. Hydroisomerization/hydrocracking process of *n*-hexadecane over bifunctional catalysts.

multi-component mixtures *i.e.* SBA-15+zeolite materials extruded with binder (here γ-Al_2O_3). It allowed to follow not only the properties of micro-mesoporous catalysts, but also to test the catalysts which were similar to the commercial catalysts, *i.e.* shaped with binder. Studies on the micro-mesoporous materials rather did not took into account that aspect. In this work micro-mesoporous support (AlSBA-15+ BEA zeolite) were impregnated with 0.5 wt% of platinum using H_2PtCl_6, Pt$(NH_3)_4(NO_3)_2$ or Pt$(NH_3)_4Cl_2$. The textural properties, metallic and acidic functions were characterized by means of N_2 sorption, XRD, TEM, FTIR, H_2 chemisorption and *Py*-FTIR. In this work consideration was given to: (*i*) the effect of Pt precursor on the dispersion and size of metal particles, (*ii*) the effect of the metal location on catalytic performance of composite catalysts.

2. Experimental

2.1. Materials

For the synthesis of bioporous materials (AlSBA-15 + BEA zeolite) and preparation of 0.5 wt% Pt supported catalysts: tetraethylorthosilicate (TEOS, 98% purity, Aldrich); Pluronic P123 (Aldrich); hydrochloric acid (HCl, 37%, Avantor) aluminium isopropoxide (IP; $[(CH_3)_2CHO]_3Al$, Acros), H-BEA zeolite (CP811E, Zeolyst, Si/Al = 75), AlO(OH) (Pural 400, Sasol GmbH, after calcination γ-Al_2O_3), nitric acid (HNO_3, 3%, Avantor), Hexachloroplatinic acid (H_2PtCl_6), tetraamminplatinum (II) nitrate (Pt$(NH_3)_4(NO_3)_2$; Sigma-Aldrich, 482293) and tetraamminoplatinum (II) chloride (Pt$(NH_3)_4Cl_2$; Sigma-Aldrich, 275905) were used.

2.2. Catalyst preparation

The synthesis of composite material AlSBA-15 + BEA zeolite (weight ratio zeolite: AlSBA-15 = 1:4) was carried out following the procedure presented in Scheme 2 and described in detail in our recent work [18].

The powder of AlSBA-15 + BEA zeolite were blended with binder - 20 wt% of AlO(OH), peptized with 3% solution of HNO_3 and then shaped into the cylindrical extrudates. The resulting extrudates were dried (12 h at 110 °C) and calcined (6 h at 450 °C). The platinum catalysts were prepared by the dry impregnation method using formed and calcined extrudates with a particle size of 0.40–0.63 mm and three different platinum precursors: H_2PtCl_6, Pt$(NH_3)_4(NO_3)_2$ and Pt$(NH_3)_4Cl_2$. For all catalysts the Pt loading was 0.5 wt%. The impregnated materials were dried overnight at RT, next 12 h at 110 °C and then calcined for 6 h at 450 °C. Following the preparation procedure described above and using three Pt precursors, *i.e.* H_2PtCl_6, Pt$(NH_3)_4(NO_3)_2$ and Pt$(NH_3)_4Cl_2$, the catalysts were designated as: Pt/SBA_BEA, Pt/SBA_BEAn and Pt/SBA_BEAc, respectively.

2.3. Catalyst characterization

2.3.1. Texture

The pore structure and Brunauer-Emmett-Teller specific surface area (S_{BET}) of Pt/AlSBA-15 + BEA were determined by nitrogen adsorption-desorption at −196 °C using Autosorb-1C Quantachrome analyzer. Before the adsorption measurements, samples were degassed for 6 h at 150 °C. Further, the samples were filled with nitrogen and analyzed for 13 h. Distribution of pore sizes was calculated according to Barrett-Joyner-Halenda method (BJH).

To confirm the ordered mesoporous structure of AlSBA-15 and crystalline structure of BEA zeolite, powder X-ray diffraction (XRD) was conducted using X'Pert Pro equipment (PANalytical) with CuKα radiation (λ = 0.154 nm, A40 kV, 40 mA). The data were collected in the range from 0.5 to 5° (2θ) and from 10 to 80° (2θ) at a scan steps of 0.026° (2θ) s^{-1}.

2.3.2. Characterization of the metallic function

Hydrogen chemisorption was performed using Micromeritics ASAP 2020. Prior to the measurement, the 25 mg of sample was reduced in situ using H_2 flow for 1 h at 450 °C. Next, the sample was cooled to 35 °C under He flow. The measurement was carried out at the pressure range from 10 to 450 Torr. The average metal particle size (d_{Pt}), metal dispersion (D) and Pt surface area (S_{Pt}) were calculated at the chemisorption stoichiometry of H:Pt = 1 based on the procedure described by Hunt et al. [43].

2.3.3. Characterization of the acidic function

Acidity of catalysts was determined using pyridine infrared spectroscopy (*Py*–FTIR). The IR spectra were measured on a Bruker Vector 22 spectrophotometer. Prior to the measurement the catalysts samples

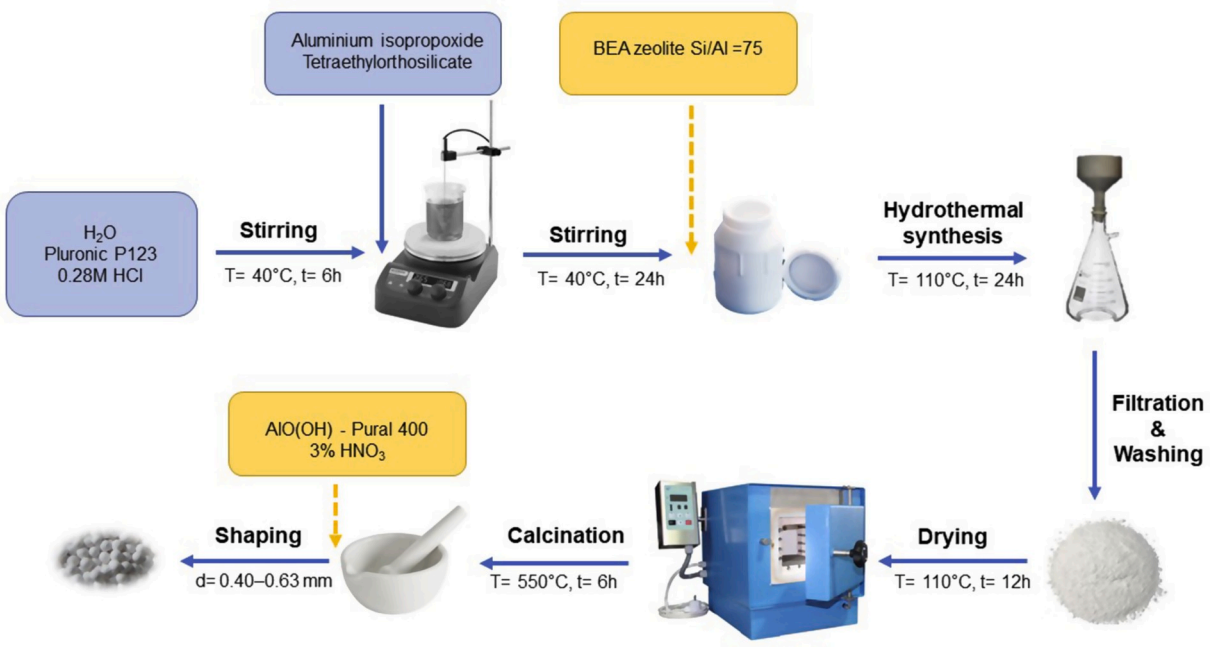

Scheme 2. Synthesis of bimodal AlSBA-15+ BEA zeolite supports.

were pressed into self-supporting wafers. Next, the tablets were placed inside the FTIR quartz chamber and degassed under vacuum for 1 h at 400 °C. Then, the samples were subsequently exposed to pyridine vapor at 150 °C. The IR spectra were then recorded at 150, 200, 250, 300 and 350 °C in vacuum for 30 min in the range from 1400 to 1700 cm^{-1}. The quantitative calculation of Brønsted and Lewis acid sites was made with respect of IR vibrational bands observed at about 1545 and 1454 cm^{-1}, respectively.

2.3.4. FTIR analysis

Prior to the analysis, samples of the Pt catalysts were dried for 24 h at 80 °C. For FTIR analysis, KBr tablets were prepared with each containing 1.5 mg of the catalysts samples and 200 mg of KBr. The spectra was recorded on a Bruker spectrophotometer (FTIR IFS 66/s) in the mid IR range (400–4000 cm^{-1}).

2.3.5. TEM

The micro-mesoporous structure of supports and distribution of Pt particles of the samples was investigated with a Hitachi H-800 microscope, operating at 150 kV. Prior to imaging, the samples were dispersed in methanol and placed on the microscope copper grid covered with a carbon film.

2.4. Catalytic experiments

The hydroisomerization of *n*-hexadecane (*n*-C_{16}) was carried out in a high-pressure stainless-steel flow reactor with a fixed catalyst bed of approximately 80 mm long. Prior to the catalytic activity test, the catalysts (1.0 g, 0.40–0.63 mm) were activated at 250 °C (1 h), 350 °C (1 h) and 450 °C (3 h) under H_2 pressure of 5 MPa. The activity test was carried out under H_2 pressure of 5 MPa, the H_2:CH molar ratio of 4.6 mol/mol, the WHSV of 3.5 h^{-1} and at the temperature range from 260 to 320 °C. The liquid products of reaction were collected at 3.5 h intervals and analyzed using the gas chromatography (PerkinElmer Clarus 580) with Elite 1 column (60 m × 0.53 mm × 1.5 μm). The total hydroisomerization reaction time on steam was 14 h. Additionally, in Supporting information a comparison results of catalytic experiments for 3 different catalysts were compared: Pt/AlSBA-15 (Pt over pure AlSBA-15 Si/Al = 7), Pt/zeolite BEA (Pt over pure BEA zeolite Si/Al = 75), and Pt/SBA_BEA(F) (composite material prepared by mechanical mixing of AlSBA-15 and BEA zeolite, AlSBA-15:zeolite = 4:1). The Pt loading was 0.5 wt% and the Pt-precursor was H_2PtCl_6.

The liquid reaction products were grouped as follows:

(i) *i*-C_{16} (hydroisomerization products), including $MoBC_{16}$ (monobranched isomers), $DiBC_{16}$ (dibranched isomers) and $MuBC_{16}$ (multibranched isomers),
(ii) C_3–C_{13} (hydrocracking products, HK),
(iii) HK_{ind} = mol of C_3–C_{13} per mol of cracked *n*-C_{16} (mol/mol), also known as CB = carbon mass balance [44].

In the case of catalysts prepared with use of different Pt precursor, hydrocarbons with 14 and 15 carbon atoms (produced in hydrogenolysis of *n*-C_{16}) were not observed among the reaction products.

In order to verify the reproducibility of the catalytic test, the experiments were repeated 2 times for all Pt catalysts. The results of reproducibility were calculated as a standard deviation and this standard deviation based on *n*-C_{16} conversion was below 1%.

3. Results and discussion

3.1. Characterization of supports and composite Pt catalysts

3.1.1. Texture of the AlSBA-15+zeolit material and the Pt/AlSBA-15+zeolit catalyst

The textural properties of Pt catalysts prepared with use of various platinum precursors are collected in Fig. 1 and in Table 1. The occurrence of the highly ordered mesoporous structure of AlSBA-15 in bimodal support was confirmed by a low-angle XRD (Fig. 1A). The presence of intense three diffraction peaks at 2θ around 0.9, 1.6 and 1.8° corresponded to (1 0 0), (1 1 0) and (2 0 0) planes in the hexagonal structure of SBA-15, respectively. It is also worth noting that in the bimodal supports, the crystalline structure of zeolite was preserved. The wide-range XRD patterns (Fig. 1B) of bimodal catalysts displayed diffraction peaks in the range of 12–14° and 22.5° (2θ) which were attributed to crystalline phase of BEA zeolite. For all catalysts the wide-range XRD patterns did not show any diffraction peak characteristic for platinum, which may be due to the low Pt loading - below than the detection limit of the XRD technique. Additionally in tested catalysts, the presence of extra crystalline lattices were not observed. It suggests, that BEA zeolite had relatively high crystallinity and the Pt species were highly dispersed on bimodal supports, as expected. Nevertheless, the intensity of reflections typical for the BEA zeolite were much lower in the bimodal materials in comparison with pure zeolite due to: (*i*) the presence of only 20 wt% of zeolite in the support and/or (*ii*) the creation of mesopores in zeolite crystals as a result of zeolite digestion by HCl at the stage of synthesis of the bimodal support.

Fig. 1C shows the low-temperature N_2 adsorption-desorption isotherms and pore size distributions of Pt catalysts. Regardless of the used Pt precursors, for all catalysts, the isotherms type IV with capillary condensation step around p/p_0 of 0.75 was observed, which is characteristic for mesoporous materials SBA-15 type. Furthermore, for all catalysts supported on AlSBA-15+ BEA zeolite, H1-type hysteresis loop was observed, which presence confirmed highly ordered mesoporous structure of the SBA-15 with double-opened cylindrical-shape pores. As was expected, all of the composite catalysts, showed lower S_{BET} and total pore volume determined at $p/p_0 > 0.99$ (V_T) in comparison with the powder of AlSBA-15 + BEA (sample designated as SBA_BEA^P, Table 1). It might due to the addition of binder during support preparation (sample designated as SBA_BEA^B, Table 1) as well as Pt deposition. Studied catalysts show the narrow pore size distribution with the maximum pore sizes were within the range of 7.4–7.7 nm (Fig. 1D). Among the catalysts, the largest S_{BET} (560 m^2 g^{-1}) and V_T (0.94 cm^3 g^{-1}) was found for Pt/SBA_BEAn prepared by impregnation with $Pt(NH_3)_4(NO_3)_2$. In the case of the Pt/SBA_BEAc prepared by impregnation with $Pt(NH_3)_4Cl_2$, a significant decrease of S_{BET} and V_T was observed in comparison with Pt/SBA_BEA and Pt/SBA_BEAn. This phenomenon was probably caused by the partial blockage of the Pt/SBA_BEAc catalyst pores by large Pt crystals (d_{Pt} about 5.1 nm).

3.1.2. Characterization of the metal function

Table 1 summarises the results of the H_2 chemisorption measurments (Pt dispersion, D; Pt particle diameter, d_{Pt}; Pt surface, SPt). Obtained data indicated, that the Pt precursor significantly affect both the dispersion and preferred adsorption of Pt particles on composite support components *i.e.* AlSBA-15, BEA zeolite or Al_2O_3, during the impregnation step. The Pt/SBA_BEA catalyst exhibited the highest Pt dispersion (58%) and the smallest particle size (2.0 nm). The Pt dispersion on the surface of catalysts obtained using $Pt(NH_3)_4(NO_3)_2$ and $Pt(NH_3)_4Cl_2$ were lower and equaled 32 and 23%, respectively. Average particle size located on Pt for Pt/SBA_BEAn and Pt/SBA_BEAc samples were much larger than for Pt/SBA_BEA catalyst and equaled 3.6 and 5.1 nm, respectively.

The reason for the differences in Pt particle size and their dispersion may be: (*i*) different values of PZC of support surface and pH of aqueous precursor solutions used for impregnation, *i.e.* 2.2; 6.0 and 6.5 for H_2PtCl_6, $Pt(NH_3)_4(NO_3)_2$, $Pt(NH_3)_4Cl_2$, respectively (Fig. 2) and (*ii*) the presence of ammonium and chlorine ions in the calcination step during catalysts preparation. The pH value at which the carrier surface is inert is termed the point of zero charge (PZC). When choosing a metal precursor and a method of metal incorporation to a supports, it is important to know the PZC value and the pH of the metal precursor solution.

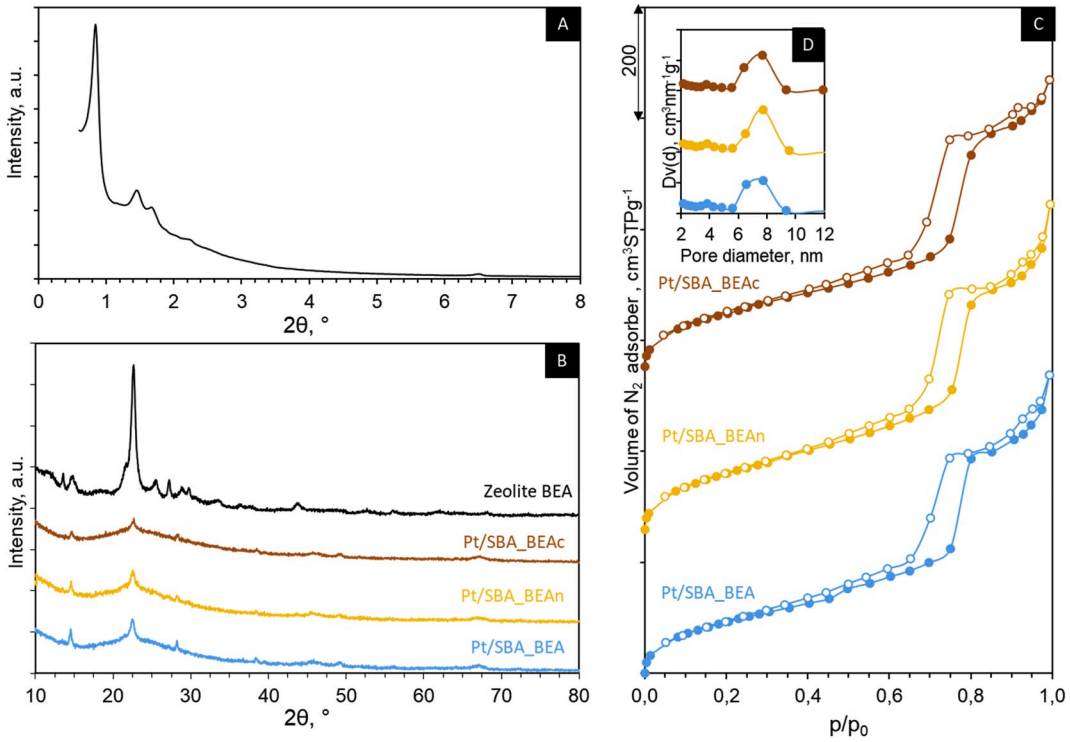

Fig. 1. Characterization of bimodal catalysts based on AlSBA-15 and zeolite BEA; A) low-angle XRD pattern, B) wide-angle XRD patterns C) N_2 adsorption-desorption isotherms and D) the pore size distributions.

Table 1
The physicochemical and chemical properties of the supports and the catalysts.

Sample	Precursor of Pt	S_{BET} ($m^2 \cdot g^{-1}$)	[a]V_T ($cm^3 \cdot g^{-1}$)	[b]S_{MES} ($m^2 \cdot g^{-1}$)	[c]V_{MES} ($cm^3 \cdot g^{-1}$)	[d]d_{BJH} (nm)	[e]D (%)	[f]S_{Pt} ($m^2 \cdot g_{cat}^{-1}$)	[g]d_{Pt} (nm)
SBA_BEA[P]	–	736	1.12	613	0.73	7.8	–	–	–
SBA_BEA[B]	–	581	0.94	480	0.59	7.8	–	–	–
Pt/SBA_BEA	H_2PtCl_6	524	0.93	302	0.51	7.7	58	144	2.0
Pt/SBA_BEAn	$Pt(NH_3)_4(NO_3)_2$	560	0.94	450	0.49	7.7	32	77	3.6
Pt/SBA_BEAc	$Pt(NH_3)_4Cl_2$	494	0.91	400	0.56	7.4	23	55	5.1

[a] V_T - total pore volume determined at $p/p_0>0.99$, [b] S_{MES} – surface of mesopore from t-plot, [c] V_{MES} - volume of mesopore from t-plot, [d] d_{BJH} - pore diameter (BJH method),[e] D - dispersion, [f] SPt - Pt surface area, [g] dPt - average Pt particle diameter, [P] powdered supports without binder, [B] supports with binder.

During the impregnation of the carrier, the hydroxyl groups located on its surface, become protonated (positively charged), or deprotonated (negatively charged) [45]. In case of impregnation with a solution with a pH value above the PZC value of the carrier, its surface will be polarized negatively and will preferentially adsorb the cations such as $[Pt(NH_3)_4]^{2+}$. Meanwhile, using the impregnating solution with a pH below the PZC of the carrier, the surface of carrier is positively charged and will adsorb anions such as $[PtCl_6]^{2-}$. In addition, the important parameter that influences the dispersion and size of metal particles is the difference between the pH value of the impregnating solution and the PZC of the carrier. Higher difference between the pH and PZC values led to the stronger precursor–carrier interactions, and as a result to a higher concentration of the active phase introduced and its better dispersion [46]. The results of Hao et al. [45], Spieker et al. [47] and Samad et al. [25] indicated, that knowing the PZC value of the carrier and using solutions of metal precursors with different pH, preferential metal deposition on a support component can be predicted. In consequence, not only the size of metal particles can be controlled, but also the ratio and proximity of the metal and acid sites.

In the case of catalysts based on a bimodal material consisting of AlSBA-15 (PZC≅ 5) [48], BEA zeolite (PZC≅ 6) [49] and Al_2O_3 (PZC≅ 8) [46] it was found, that the high difference between the pH value of the H_2PtCl_6 solution (pH = 2.2) and the pH PZC value of all support components, promoted adsorption of $[PtCl_6]^{2-}$ ions on its surface. Meanwhile, the higher pH values of $Pt(NH_3)_4(NO_3)_2$ (pH = 6) and $Pt(NH_3)_4Cl_2$ (pH = 6.5) solutions and lack or small differences in their pH values, with respect to PZC value of the support components, were the cause of weaker interactions between the $[Pt(NH_3)_4]^{2+}$ ions and the carrier surface. Reduction of the strength of metal - support interactions in contrast led to decrease of metal dispersion and the increase in Pt crystals size (Table 1). Hence, Pt dispersion on the Pt/SBA_BEA catalyst was about 1.8 and 2.5 fold higher, than on the Pt/SBA_BEAn and Pt/SBA_BEAc, respectively. On the other hand, the use of cationic Pt precursors allowed to incorporate platinum into the zeolite and reduction of the proximity of acid and metallic sites. Thus, it appears, that in cases of impregnation of carriers containing zeolite, the usage of precursors such as $Pt(NH_3)_4(NO_3)_2$ and $Pt(NH_3)_4Cl_2$ was reasonable, because the incorporation of Pt around the acid sites was enabled. However, the incorporation of Pt into the zeolite crystals through ion exchange, disabled determination of Pt dispersion using chemisorption method. This phenomenon was confirmed by Wang et al. [19] and Geng et al. [39], who observed that not all Pt particles located on zeolite crystals are occupied by adsorbed CO or H_2 molecules and may negatively affect the chemisorption results – decrease Pt dispersion and increase the size of Pt crystals in comparison with the real values. As was earlier mentioned, the presence of chlorine ions in the Pt precursor

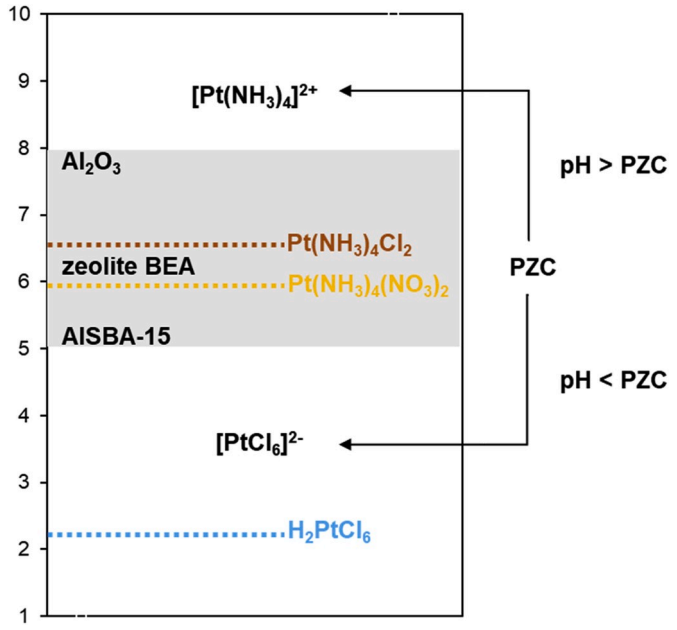

Fig. 2. Electrostatic adsorption mechanism of Pt ions on bimodal supports consisting of AlSBA-15, BEA zeolite and Al_2O_3.

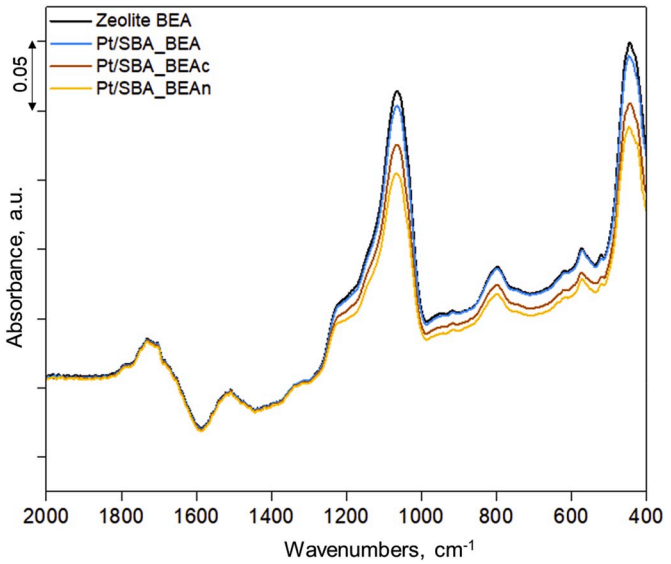

Fig. 3. FTIR spectra of zeolite BEA and Pt/SBA_BEA, Pt/SBA_BEAn and Pt/SBA_BEAc catalysts obtained by impregnation with different Pt precursors.

impacts the metal dispersion. As it was described by Kanda et al. [50] and Jaroszewska et al. [51], the interactions between the chlorine residues and Al phase were stronger than the ones between the chlorine residues and Si species. Therefore, the chlorine containing precursors should be preferably adsorbed on the Al-rich surfaces; in the case of investigated here catalysts on Al_2O_3 binder. Nevertheless our results proved, that in the case of the catalyst impregnated with H_2PtCl_6 solution, Pt was located mainly over the AlSBA-15 surface (Fig. 4A). We believe, that in can be linked with some structural effect *i.e.* high surface area of AlSBA-15 and the presence of 80 wt% AlSBA-15 in the catalyst composition. In consequence, it can be expected, that the dispersion of Pt on AlSBA-15 will be high and a good Pt dispersion may provide high catalytic activity. However, the presence of Pt species located on Al_2O_3 cannot be neglected because these Pt species can be involved in a sufficient delivery of spillover hydrogen onto the acid sites of AlSBA-15 and zeolite components. It is also known the role of chlorine ions in preserving Pt dispersion in reforming catalysts [52]. The chlorine ions react with oxidized Pt species distributed over the Al_2O_3 support to form mobile platinum oxychloride $[Pt_{IV}O_xCl_y]_s$, which redistributes the Pt over the catalysts support. Chlorine ions are required for re-dispersion of the Pt atoms in spent catalysts but also to help maintain a high Pt dispersion during the process. The decomposition of ammonium ions during catalyst calcination leads to the release of ammonia and subsequently to remaining a proton on the surface (acid form of AlSBA-15 and/or zeolite). Calcination of the chlorine-containing precursor does not lead to its removal from the surface - Cl remains on it, *e.g.* bound to alumina or in the acid center of zeolite. Each time it causes changes in concentration, strength and distribution of acid centers on the surface (to vary degrees for individual carrier components).

3.1.3. FTIR and TEM measurements

In Fig. 3, the FTIR absorption spectra of pure zeolite and bimodal catalysts are presented. For all samples the FTIR spectrum contains a group of absorption bands with a high intensity in the range from 1750 to 400 cm^{-1}. The peaks at around 570 and 445 cm^{-1} indicate the presence of five-membered double rings, typical for BEA zeolite and were assigned to the internal flexions of T–O–T (where T symbolizes the atom of Si or Al) siloxane bonds in the rings [53,54]. The peak at 800 cm^{-1}, was attributed to symmetric stretching vibrations of the siloxane groups, from internal bonds of the tetrahedral SiO_4 structural unit. The signals at around 1090 and 1200 cm^{-1} were assigned to internal asymmetric stretching vibrations of the T-O-T bond and external asymmetric stretching vibrations of T-O-T, respectively [55]. For all samples, the signals at approximately 1500 and 1700 cm^{-1} may correspond to the deformational vibrations of water trapped in the pores of materials.

It is also worth noting that in FTIR absorption spectra for both Pt/SBA_BEAc and Pt/SBA_BEAn, a significant decline in the intensity of the main peaks corresponding to T-O-T vibrations in the zeolite skeleton was observed. It might be a result of the deposition of Pt on zeolite crystals caused by partial ion exchange. Jin et al. [56] and Gülec et al. [54] observed, that during the impregnation with aqueous metal precursor solutions, the partial ion exchange in zeolites occurs.

In order to further investigate the impact of Pt precursor on the platinum particle size and their location on the support, Pt catalysts were examined by means of TEM. The TEM micrographs of the catalysts are given in Fig. 4. On all TEM micrographs of bimodal catalysts, it can be observed, that the size of BEA zeolite crystals varied from 50 to 200 nm. However, it should be noted, that for some crystals their edges were not regular, which indicates the partial change of their structure. This phenomenon might be caused by interaction with the HCl solution during the synthesis of bimodal material - formation of secondary porosity within. Hence, in some of BEA zeolite crystals, the presence of randomly distributed mesopores can be observed. Additionally, TEM micrographs of Pt/SBA_BEAn and Pt/SBA_BEAc (Fig. 4C and F) demonstrated uniform and hexagonally ordered SBA-15-type mesostructure. In Fig. 4 A,C,E, also some areas of amorphous materials derived from the binder (Pural 400) were observed. Also in the case of catalysts obtained by impregnation with an aqueous solutions of Pt $(NH_3)_4Cl_2$ and $Pt(NH_3)_4(NO_3)_2$, the Pt particles were mainly located on zeolite crystals (Fig. 4C-F). In contrast to the catalysts obtained by impregnation with solution containing $[Pt(NH_3)_4]^{2+}$ ions, the usage of solution containing $[PtCl_6]^{2-}$ ions allowed Pt to be deposited mainly on AlSBA-15 (80% of the mass of the supports with ratio AlSBA-15:zeolite = 4:1), thus better dispersion of Pt particles and smaller particle size was obtained (Fig. 4A). The TEM micrograph of Pt/SBA_BEAn and Pt/SBA_BEAc exhibited, that the average diameter of Pt particles on these catalysts was larger than that for the Pt/SBA_BEA catalyst. Both, TEM micrographs and H_2 chemisorption, implied that the diameter of Pt particles on catalysts obtained by impregnation with cationic Pt precursor, was larger, what might be a result of autoreduction of Pt by NH_3,

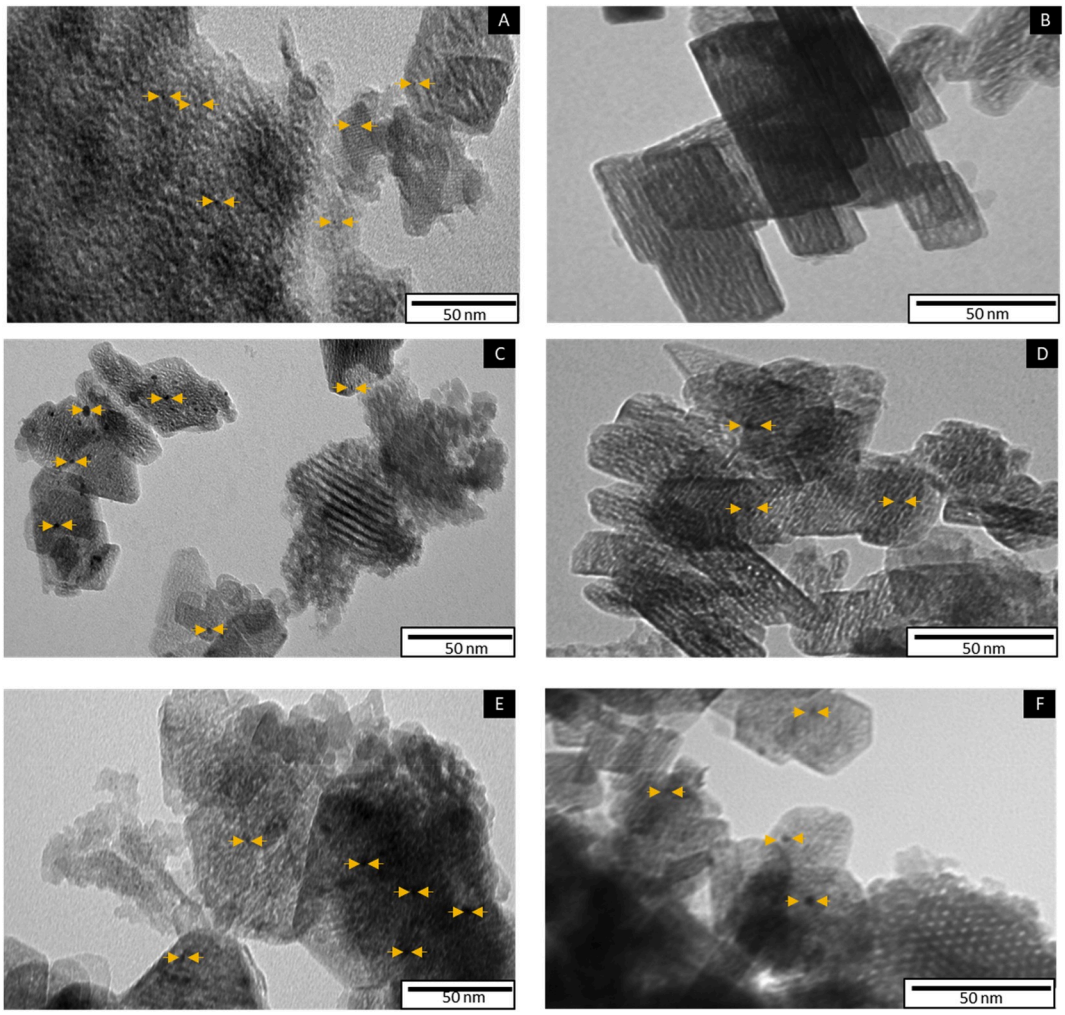

Fig. 4. TEM images of A-B) Pt/SBA_BEA, C-D) Pt/SBA_BEAn and E-F) Pt/SBA_BEAc catalysts.

during calcinations process. On the other hand, the usage of $Pt(NH_3)_4Cl_2$ and $Pt(NH_3)_4(NO_3)_2$ for impregnation of the composite support, allowed to reduce the distance between the metal and Brønsted acid sites present in zeolite in comparison with the Pt(0.5) SBA_BEA catalyst. Considering the points of zero charge of individual support components, *i.e.* BEA zeolite (PZC≅ 6), AlSBA-15 (PZC≅ 5) and Al_2O_3 (PZC≅ 8) and results of H_2 chemisorption, FTIR and TEM it can be stated that in the case of composite catalysts, the usage of different Pt precursors can influence the location of Pt particles and their size, thereby controlling the distance of acid and metallic sites.

3.1.4. Acidity of the catalysts

The *Py*–FTIR spectra of pyridine desorption at 150 °C of the calcined and reduced Pt catalysts are shown in Fig. 5A. The quantitatively calculated values from the *Py*–FTIR spectra of pyridine desorption at 150, 250 and 350 °C in the range of 1700–1400 cm^{-1} were compared in Table 2 and Fig. 5B and C. For all samples, pyridine absorption bands attributed to both Lewis and Brønsted acid sites were observed. Peaks at wavelength of 1623 and 1454 cm^{-1} were assigned to pyridine coordinated to the Lewis acid sites and the bands at 1635 and 1545 cm^{-1} were attributed to pyridine bounded to the Brønsted acid sites. The peak at 1490 cm^{-1} can be assigned to pyridine associated with both Brønsted and Lewis acid sites [57]. *Py*–FTIR measurements revealed that for all investigated Pt catalysts, the concentration of Brønsted acid sites was higher than the concentration of the Lewis acid sites (Fig. 5. B and C). On the other hand, for all catalysts the strength of Brønsted acid sites was much lower than the strength of Lewis acid sites. In the case of composite Pt catalysts consisting of AlSBA-15, BEA zeolite and γ-Al_2O_3 (a binder), the Lewis acid sites might be generated on the surface of each ingredients - Al in extra framework positions (AlO_6 structural unit). The presence of Brønsted acid sites was associated with the acidity of zeolite and AlSBA-15 material - in which Al was covalently bounded with four Si atoms *via* oxygen bridges (AlO_4 structural unit). The concentration of Brønsted acid sites depends also on the presence of chlorine ions from either decomposition of Pt precursor *e.g.* H_2PtCl_6 and/or HCl used in the synthesis AlSBA-15. The results of Wang et al. [19] also showed that the deposition of platinum on the surface of the support may modify its acid function as a result of coating some of the acid sites arranged on its surface with platinum particles - Pt particles covered both Brønsted and Lewis acid sites. On the other hand, the results of Fang et al. [58] revealed, that Pt-supported atoms can form additional Lewis acid sites. Thus, the effect of "*reducing the concentration of Lewis acid sites*", caused by covering of Lewis acid sites by Pt was reduced.

The total concentration of acidic sites on the surface of catalysts with different Pt precursor decreases in the following order: Pt/SBA_BEAc > Pt/SBA_BEA > Pt/SBA_BEAn. In contrast, the ratio of the Brønsted acid sites concentration to the total Brønsted and Lewis acid sites concentration increased in the order Pt/SBA_BEAc ≈ Pt/SBA_BEAn < Pt/SBA_BEA (Table 2, ratio $\frac{PyH+}{PyH++PyL}$). This phenomenon remained in correlation with the increase in Pt dispersion on these catalysts (Table 1). Thus, the concentration of Brønsted acid sites on the surface of the catalysts also depended on the dispersion of the metallic phase.

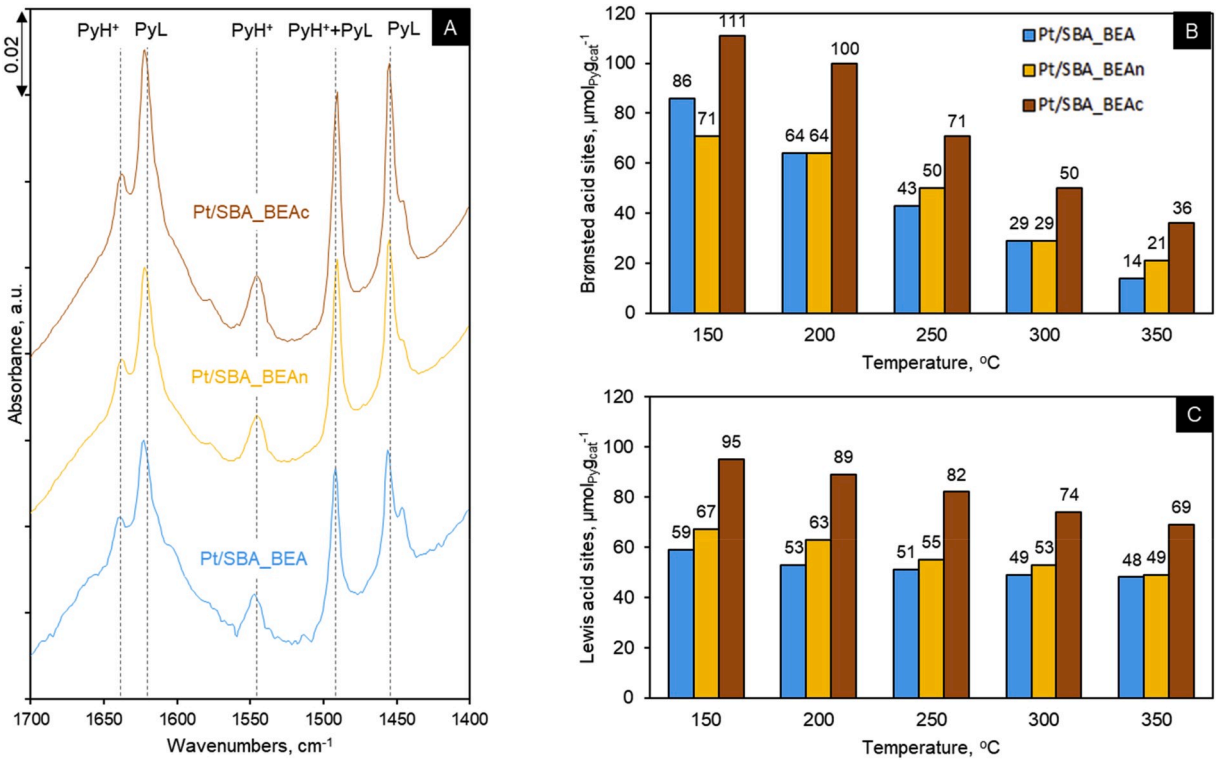

Fig. 5. A) FTIR spectra of pyridine adsorbed on Pt/SBA_BEA, Pt/SBA_BEAn and Pt/SBA_BEAc catalysts at temperature 150 °C; PyH^+- Brønsted acid sites; PyL- Lewis acid sites. B and C) Distribution of acid sites strength of Pt catalysts by Py-FTIR (μmol$_{Py}$g^{-1}).

Table 2
The acidic properties of Pt catalysts by *Py*-FTIR (μmol$_{Py}$g^{-1}).

Sample	PyH^+ A_{350}/A_{150}[a]	PyL A_{350}/A_{150}[b]	$PyH^+ + PyL$[c]	$\frac{H+}{H++L}$[d]
Pt/SBA_BEA	0.16	0.81	145	0.60
Pt/SBA_BEAn	0.30	0.73	138	0.51
Pt/SBA_BEAc	0.32	0.72	206	0.54

[a] The strength of the Brønsted acid sites calculated as ratio of relevant peaks intensities.
[b] The strength of the Lewis acid sites calculated as ratio of relevant peaks intensities.
[c] Total acidity defined as the concentration of pyridine molecules retained on both Brønsted and Lewis acid sites after outgassing at 150 °C.
[d] The ratio of the Brønsted acid sites concentration to the total Brønsted and Lewis acid sites concentration.

Additionally, the $\frac{nPt}{n\Sigma Py-IR}$ ratio was calculated to evaluate the balance between metal and acid sites in the catalysts for hydroisomerization of *n*-alkanes. The obtained results were presented in Table 2. We observed significant differences in the values of $\frac{nPt}{n\Sigma Py-IR}$ ratio among the three samples. The ratio decreased in order: Pt/SBA_BEA ($\frac{nPt}{n\Sigma Py-IR} = 0.10$) > Pt/SBA_BEAn ($\frac{nPt}{n\Sigma Py-IR} = 0.06$) > Pt/SBA_BEAc ($\frac{nPt}{n\Sigma Py-IR} = 0.03$). Pt/SBA_BEA and Pt/SBA_BEAn were characterized by comparable concentration of total acid sites, thus the differences in ratio value was a result of various Pt dispersion (58% for Pt/SBA_BEA and 35% for Pt/SBA_BEAn). On the other hand, for Pt/SBA_BEAc low value of ratio was a result of: high concentration of acid sites *i.e.* 206 μmolPyg^{-1}, and low amount of accessible Pt atoms (dispersion of 23%). However, there are many works [10,59] on hydroisomerization of *n*-alkanes on bifunctional catalysts, where it was proved, that one metal site could balance even few acid sites. This phenomenon allows to explain how at such great differences in $\frac{nPt}{n\Sigma Py-IR}$ ratio values for examined catalysts it is possible to achieve balance between the concentration of metal and acid sites.

3.2. Catalytic test

Hydroisomerization of *n*-C_{16} was selected to evaluate the catalytic performances of bifunctional catalysts studied in this research. The conversions of *n*-C_{16} over Pt/SBA_BEA, Pt/SBA_BEAn and Pt/SBA_BEAc are illustrated in Fig. 6 as a function of temperature. The distribution of the reaction products as a function of temperature and conversion is plotted in Figs. 6 and 7. It was observed, that activity and selectivity to C_{16} isomers of studied catalysts depended not only on the reaction temperature but also on the Pt precursor used for catalyst preparation. For all catalysts the activities increased with rise of the temperature from 260 to 320 °C, providing *n*-C_{16} conversion in the range of 8–97%. Irrespective on reaction temperature, the activity of the catalysts decreases in following Pt/SBA_BEA ≈ Pt/SBA_BEAn > Pt/SBA_BEAc, what suggests that conversion of *n*-C_{16} was not dependent only on the Pt dispersion (Table 1), but also on the concentration of acid sites and $\frac{nPt}{n\Sigma Py-IR}$ ratio (Table 2 and Fig. 5B and C). In the case of Pt/SBA_BEA catalyst the higher dispersion of Pt particles resulted in the creation of a large number of active metallic sites ($\frac{nPt}{n\Sigma Py-IR} = 0.10$), which consequently led to the formation of a large amount of intermediates as a result of dehydrogenation of the *n*-alkane. On the other hand, the useage of a Pt/SBA_BEAn catalyst, where Pt particles were deposited on zeolite crystals (in spite of lower dispersion of 32%), ensured smaller distance between acid and metal sites. This phenomenon, might increase the number of intermediates and improve the transfer of intermediates that took place between the two active sites. Among the examined catalysts, Pt/SBA_BEAc ($\frac{nPt}{n\Sigma Py-IR} = 0.03$) was less active, when compared to both others and required higher reaction temperature to ensure comparable conversion level (Fig. 6a). It appeared, that in the case of Pt/SBA_BEAc, the deposition of Pt particles on BEA zeolite crystals (Fig. 4E) did not increase its activity, which may be due too low Pt dispersion (D = 23%), large Pt particle size (d_{Pt} = 5.6 nm) and low $\frac{nPt}{n\Sigma Py-IR}$ ratio value.

For all investigated catalysts, the *n*-C_{16} conversion led to the

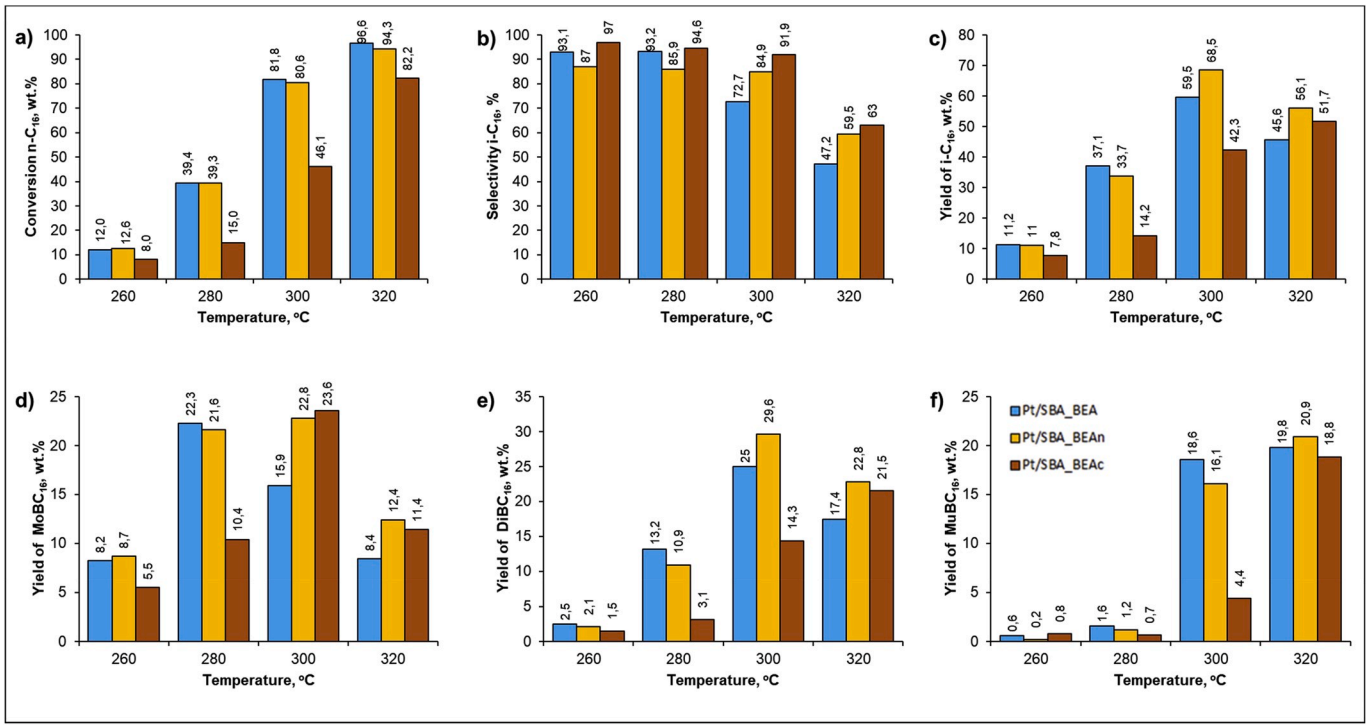

Fig. 6. (a) *n*-C_{16} conversion; (b) selectivity *i*-C_{16}; (c) yield of *i*-C_{16}; (d) yield of monobranched ($MoBC_{16}$) isomers; (e) yield of dibranched ($DiBC_{16}$) isomers and (f) yield of multibranched ($MuBC_{16}$) isomers.

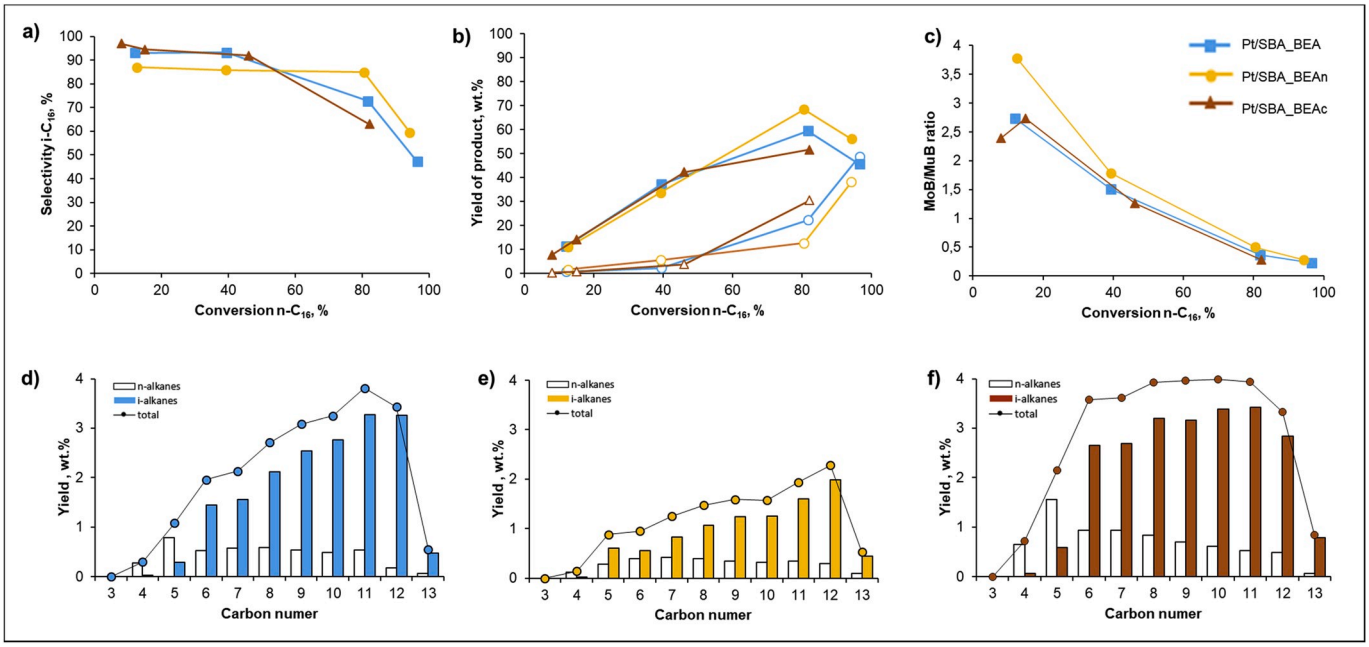

Fig. 7. (a) Selectivity of i-C_{16}, (b) yield of i-C_{16} (filled symbol) and cracking products HK (empty symbol), (c) ratio of MoB/MuB isomers of C_{16}, (d–e) distribution of hydrocracking products by carbon number at 80% conversion of *n*-C_{16} for catalysts Pt/SBA_BEA, Pt/SBA_BEAn and Pt/SBA_BEAc, respectively.

formation of hydroisomerization products and at higher reaction temperatures also hydrocracking products (Figs. 6 and 7). It was observed, that with the increase of reaction temperature, the yield of isomers increased and passed through the maximum at conversion of *n*-C_{16} around 80% and then decrease. For Pt/SBA_BEA and Pt/SBA_BEAn maximum yield of *i*-C_{16} equaled 59 and 68 wt%, respectively (Figs. 6c and 7b). While, the maximum yield of isomers on Pt/SBA_BEAc was 51 wt% with 82% of total *n*-C_{16} conversion at 20 °C higher temperature compared to the other two catalysts (Figs. 6c and 7b).

In Fig. 7a, the relationship between the selectivity of *i*-C_{16} and conversion of *n*-hexadecane was presented. The selectivity of *i*-C_{16} over the three catalysts decreased with the increase of conversion. Among of three Pt catalysts, at *n*-C_{16} conversion <50%, Pt/SBA_BEA and Pt \SBA_BEAc showed the highest selectivity (S_{HI} > 90%). This phenomenon was caused by the highest Pt dispersion *i.e.* 58% (Table 1) and $\frac{nPt}{n\Sigma Py-IR}$ ratio (Table 2) for Pt/SBA_BEA. The higher the number of

hydrogenating sites, the greater the chance for hydrogenation of isomerization products and limitation of the further cracking of the carbenium ions on the acid sites. We suppose that the high selectivity of Pt/SBA_BEAc results from not only the favourable distribution of the acidic sites on the catalyst surface, but also from the decreased distance between metallic and acid sites. However, it was observed, that in the case of both Pt/SBA_BEA and Pt/SBA_BEAc the selectivity decreased significantly with the increase of *n*-C_{16} conversion. Whereas for Pt/SBA_BEAn the isomerization selectivity was lower and remained constant *i.e.* 85% (Rys. 6b and 7a) in wider conversion range. It might be concluded, that for Pt/SBA_BEAn the better balance between metal and acid functions was obtained ($\frac{nPt}{n_{PyH+}}$=0.12).

For all catalytic systems, the main *i*-C_{16} products were $MoBC_{16}$ and DiC_{16}, which are important components of diesel fuel, due to the high cetane number and good low temperature properties (Fig. 6d and e). The yields of $MoBC_{16}$ + DiC_{16} isomers at comparable values of conversion (in our case at about 80%) equaled: 32.9, 40.9 and 52.4 wt% for Pt/SBA_BEAc, Pt/SBA_BEA and Pt/SBA_BEAn, respectively. On the other hand, the maximum yield of $MoBC_{16}$ was obtained at various temperatures and *n*-C_{16} conversion. For Pt/SBA_BEA and Pt/SBA_BEAc catalysts, the maximum yield of $MoBC_{16}$ equaled 22.3 wt% (at 39.4% of total *n*-C_{16} conversion) and 23.6 wt% (at 46.6% of total *n*-C_{16} conversion), respectively. Meanwhile, for Pt/SBA_BEAn, the maximum yield of $MoBC_{16}$ equaled 22.8 wt% (at 80.6% of total *n*-C_{16} conversion). It should be noted that the Pt/SBA_BEAn catalyst ensured high $MoBC_{16}$ yield (approx. 22 wt%) at low and high *n*-C_{16} conversions (Fig. 6a–d), which may be a result of short distance between the metallic and acidic sites and consequently fast hydrogenation of isomerization products.

For all tested catalysts, at the conversion higher than 80%, the yield of multibranched isomers of hexadecane ($MuBC_{16}$) increased. Among multibranched isomers, the main fraction were those with two methyl groups ($DiBC_{16}$). The molar ratio of monobranched to multibranched hexadecane isomers (MoB/MuB) as a function of conversion of *n*-C_{16} is shown in Fig. 7c. In all cases, the MoB/MuB ratio decreased with the increase of *n*-C_{16} conversion, which corresponds to the *n*-alkanes monomolecular isomerization mechanism *via* the protonated cyclopropane (PCP) [60]. At the same conversion (*ca.* 80%), the MoB/MuB ratio decreased in the sequence Pt/SBA_BEAn > Pt/SBA_BEA ≈ Pt/SBA_BEAc, which might be a result of different distance between metallic and acidic sites (Fig. 7c).

In the case of the tested catalysts, the isomerization was proceeded through branching from *n*-C_{16} to MoB- and further to MuB hexadecane isomers. High MoB/MuB ratio obtained for the Pt/SBA_BEAn catalyst confirmed shorter residence time of the intermediate carbenium ions on the acid sites in comparison to Pt/SBA_BEA and Pt/SBA_BEAc catalysts. Thus, the usage of catalyst obtained by impregnation with Pt$(NH_3)_4(NO_3)_2$ allowed formation of greater amount of monobranched carbenium ions, that can be transferred to the metal sites without being further branched.

It is worth to mention, that in the whole temperature range of the reaction, on the all catalysts, the yield of isomers was much higher than yield of cracking products (Figs. 6 and 7). The yields of cracked products as a function of conversion are given in Fig. 7b. The values of yields C_3–C_{13} fraction on Pt/SBA_BEAn (Fig. 7e) and Pt/SBA_BEAc (Fig. 7f) catalysts were lower than on the Pt/SBA_BEA (Fig. 7d) and increased from 0.3 to 38.2 wt%. The yield of C_3–C_{13} hydrocarbons on the Pt/SBA_BEA, varied between 0.8 and 48.8 wt%, what may be due to the greater distance between the metal and acid sites on the catalyst surface. The C_3–C_{13} fraction produced on the studied catalysts consisted mainly of *i*-alkanes (see *i*/*n* ratio in Fig. 7d–e). The values of *i*/*n* ratio for fraction C_3–C_{13} varied from 2.2 to 3.9 which corresponded to β-scissions of alkylcarbenium ions in agreement with degradation reaction type B and/or type C [18].

The distribution of the cracking products, according to the carbon numbers at conversion of *ca.* 80% is given in Fig. 7d–f. On the catalysts prepared *via* impregnation with solutions containing $[Pt(NH_3)_4]^{2+}$ ions, the distribution of cracked products was almost symmetrical with the maximum positioned at C_8 (in Fig. 7e–f). The symmetrical distribution of C_3–C_{13} fraction was observed for both catalysts and indicated the lack or very small extent of secondary cracking. However, it should be noted, that on the Pt/SBA_BEAc catalyst, the yield of cracking products was about 2-fold higher than on the Pt/SBA_BEAn, what may be due to lower activity of this catalyst ($\frac{nPt}{n\Sigma Py-IR} = 0.03$). Pt/SBA_BEAc catalyst achieved a comparable level of conversion as Pt/SBA_BEAn did at higher reaction temperature, thus the probability of hydrocarbon cracking increased. Meanwhile, the distribution pattern obtained on the Pt/SBA_BEA catalyst (in Fig. 7d) was slightly shifted towards hydrocarbons containing C_{10}–C_{12} of carbon numbers. In the case of $[Pt(NH_3)_4]^{2+}$ ions derived catalysts, lack of hydrogenolysis products, symmetrical distribution of C_3–C_{13} hydrocarbons and calculated HK_{ind} values close to 2 (ratio of the moles of cracking products to the moles of cracked *n*-C_{16}) excluded the formation of hydrocarbons during secondary cracking.

To summarize, the activity of the studied catalysts is a function of many factors (type of precursor, size and location of Pt crystallites, texture of the support, type, concentration and strength of acid sites on its surface and distance between metallic and acidic sites, pH of the impregnation solution and surface PZC). The application of the Pt/SBA_BEAn catalyst in *n*-C_{16} hydroisomerization, provided the highest yield of isomers and simultaneously, the lowest yield of cracking products. The best catalytic properties of Pt/SBA_BEAn was a result of moderate acidity, sufficient Pt distribution and privileged location of Pt species on zeolite crystals in AlSBA-15 + BEA material. Thus, the distance between metal and acid sites was reduced.

4. Conclusions

The Pt catalysts prepared by impregnation of bimodal supports using H_2PtCl_6, $Pt(NH_3)_4Cl_2$ and $Pt(NH_3)_4(NO_3)_2$. The TEM, H_2 chemisorption, FTIR and *Py*-FTIR results indicated, that the Pt distribution (dispersion, localization of Pt particles and their size) were affected by the used metal precursor. Usage of H_2PtCl_6 enabled the deposition of Pt particles mainly on the AlSBA-15 and Al_2O_3 surface. For catalysts obtained from cationic Pt precursors *i.e.* $Pt(NH_3)_4Cl_2$ and $Pt(NH_3)_4(NO_3)_2$, metal particles were distributed mainly over the zeolite crystals.

The activity and selectivity to hydroisomerization products of studied catalysts was affected by the distribution of Pt sites, which directly depended on: (*i*) PZC value of the support, (*ii*) location of Pt in cationic or anionic group, (*iii*) presence of chlorine or ammonia in precursor of Pt.

In the case of the composite support, in which each components shows different PZC, by choosing the Pt precursor (Pt in cationic or anionic group) and knowing its solution pH, it is possible to selectively incorporate the Pt particles over the surface of one of the components of the support.

The catalyst prepared with anionic precursor (H_2PtCl_6) was characterized by high activity in hydroisomerization of *n*-C_{16}, due to smaller Pt particle size and higher dispersion in comparison with the catalysts prepared with cationic Pt precursors. It appeared, that the presence of chlorine in platinum precursor, prevented Pt autoreduction during the calcination. While the usage of the precursors containing NH_3 or NH_3 and Cl simultaneously caused agglomeration of Pt sites on the catalysts surface. Despite the high catalytic activity of Pt/SBA_BEA, the maximum *i*-C_{16} yield (including desirable $MoBC_{16}$) obtained using this catalyst was lower than yield of *i*-C_{16} achieved on the Pt/SBA_BEAn catalyst. In addition, the amount of C_3–C_{13} hydrocarbons formed using Pt/SBA_BEA catalyst was significantly higher than for the catalysts obtained by impregnation with solutions containing $[Pt(NH_3)_4]^{2+}$ ions. This phenomenon resulted from the greater distance between metallic and acidic sites. It appeared, that the monobranched alkenes were formed on acidic sites, while diffusion into metallic sites, encountered several acid sites

on their way. As a result, they were transformed into multibranched alkenes and hydrocarbons containing from 3 to 13 carbon atoms.

It was observed, that the catalytic activity, yield and distribution of hydroisomerization products, strongly depended on the Pt precursor used for catalyst preparation. The catalyst prepared with use Pt $(NH_3)_4(NO_3)_2$, enabled Pt deposition ovn the BEA zeolite, reducing the distance between the metallic and acidic sites. As a result, *n*-hexadecane hydroconversion activity and isomerization selectivity were improved.

Declaration of competing interest

The authors declare that they have no known competing financial interests or personal relationships that could have appeared to influence the work reported in this paper.

Acknowledgements

This work was financed by a statutory subsidy from the Polish Ministry of Science and Higher Education, for the Faculty of Chemistry of Wrocław University of Science and Technology.

Appendix A. Supplementary data

Supplementary data to this article can be found online at https://doi.org/10.1016/j.micromeso.2020.110366.

References

[1] H. Ling, Q. Wang, B. xian Shen, Hydroisomerization and hydrocracking of hydrocracker bottom for producing lube base oil, Fuel Process. Technol. 90 (2009) 531–535, https://doi.org/10.1016/j.fuproc.2009.01.006.

[2] F. Regali, L.F. Liotta, A.M. Venezia, V. Montes, M. Boutonnet, S. Järås, Effect of metal loading on activity, selectivity and deactivation behavior of Pd/silica-alumina catalysts in the hydroconversion of n-hexadecane, Catal. Today (2014), https://doi.org/10.1016/j.cattod.2013.08.028.

[3] A. Dhar, R.L. Vekariya, P. Sharma, Kinetics and mechanistic study of n-alkane hydroisomerization reaction on Pt-doped γ-alumina catalyst, Petroleum 3 (2017) 489–495, https://doi.org/10.1016/j.petlm.2017.02.001.

[4] F. Bauer, K. Ficht, M. Bertmer, W.D. Einicke, T. Kuchling, R. Gläser, Hydroisomerization of long-chain paraffins over nano-sized bimetallic Pt-Pd/H-beta catalysts, Catal. Sci. Technol. 4 (2014) 4045–4054, https://doi.org/10.1039/c4cy00561a.

[5] B. Creton, C. Dartiguelongue, T. De Bruin, H. Toulhoat, Prediction of the cetane number of diesel compounds using the quantitative structure property relationship, Energy Fuels 24 (2010) 5396–5403, https://doi.org/10.1021/ef1008456.

[6] C. Martínez, A. Corma, Inorganic molecular sieves: preparation, modification and industrial application in catalytic processes, Coord. Chem. Rev. 255 (2011) 1558–1580, https://doi.org/10.1016/j.ccr.2011.03.014.

[7] C. Kordulis, K. Bourikas, M. Gousi, E. Kordouli, A. Lycourghiotis, Development of nickel based catalysts for the transformation of natural triglycerides and related compounds into green diesel: a critical review, Appl. Catal. B Environ. 181 (2016) 156–196, https://doi.org/10.1016/j.apcatb.2015.07.042.

[8] A. Sonthalia, N. Kumar, Hydroprocessed vegetable oil as a fuel for transportation sector: a review, J. Energy Inst. 92 (2019) 1–17, https://doi.org/10.1016/j.joei.2017.10.008.

[9] H.L. Coon Radt, W.E. Garwood, Mechanism of hydrocracking, Ind. Eng. Chem. Process Des. Dev. 3 (1964) 38–45, https://doi.org/10.1021/i260009a010.

[10] F. Alvarez, F.R. Ribeiro, G. Perot, C. Thomazeau, M. Guisnet, Hydroisomerization and hydrocracking of alkanes. 7. Influence of the balance between acid and hydrogenating functions on the transformation of n-decane on PtHY catalysts, J. Catal. 162 (1996) 179–189, https://doi.org/10.1006/jcat.1996.0275.

[11] H. Deldari, Suitable catalysts for hydroisomerization of long-chain normal paraffins, Appl. Catal. Gen. 293 (2005) 1–10, https://doi.org/10.1016/j.apcata.2005.07.008.

[12] N. Batalha, L. Pinard, C. Bouchy, E. Guillon, M. Guisnet, N-Hexadecane hydroisomerization over Pt-HBEA catalysts. Quantification and effect of the intimacy between metal and protonic sites, J. Catal. 307 (2013) 122–131, https://doi.org/10.1016/j.jcat.2013.07.014.

[13] J.E. Samad, J. Blanchard, C. Sayag, C. Louis, J.R. Regalbuto, The controlled synthesis of metal-acid bifunctional catalysts: the effect of metal:acid ratio and metal-acid proximity in Pt silica-alumina catalysts for n-heptane isomerization, J. Catal. 342 (2016) 203–212, https://doi.org/10.1016/j.jcat.2016.08.004.

[14] W. Wang, C.-J. Liu, W. Wu, Bifunctional catalysts for the hydroisomerization of n -alkanes: the effects of metal–acid balance and textural structure, Catal. Sci. Technol. (2019), https://doi.org/10.1039/c9cy00499h.

[15] A.M. Venezia, R. Murania, V. La Parola, B. Pawelec, J.L.G. Fierro, Post-synthesis alumination of MCM-41: effect of the acidity on the HDS activity of supported Pd catalysts, Appl. Catal. Gen. 383 (2010) 211–216, https://doi.org/10.1016/j.apcata.2010.06.001.

[16] P. Mäki-Arvela, D.Y. Murzin, Effect of catalyst synthesis parameters on the metal particle size, Appl. Catal. Gen. 451 (2013) 251–281, https://doi.org/10.1016/j.apcata.2012.10.012.

[17] L. Gao, Z. Shi, U.J. Etim, P. Wu, D. Han, W. Xing, S. Mintova, P. Bai, Z. Yan, Beta-MCM-41 micro-mesoporous catalysts in the hydroisomerization of n-heptane: definition of an indexed isomerization factor as a performance descriptor, Microporous Mesoporous Mater. 277 (2019) 17–28, https://doi.org/10.1016/j.micromeso.2018.10.015.

[18] K. Jaroszewska, M. Fedyna, J. Trawczyński, Hydroisomerization of long-chain n-alkanes over Pt/AlSBA-15+zeolite bimodal catalysts, Appl. Catal. B Environ. 255 (2019), https://doi.org/10.1016/j.apcatb.2019.117756.

[19] Y. Wang, Z. Tao, B. Wu, J. Xu, C. Huo, K. Li, H. Chen, Y. Yang, Y. Li, Effect of metal precursors on the performance of Pt/ZSM-22 catalysts for n-hexadecane hydroisomerization, J. Catal. 322 (2015) 1–13, https://doi.org/10.1016/j.jcat.2014.11.004.

[20] J. Kim, W. Kim, Y. Seo, J.C. Kim, R. Ryoo, N-Heptane hydroisomerization over Pt/MFI zeolite nanosheets: effects of zeolite crystal thickness and platinum location, J. Catal. (2013), https://doi.org/10.1016/j.jcat.2013.02.015.

[21] H. Ma, P. Wang, C. Wang, G. Lv, W. Qu, Z. Tian, K. Chi, H. Liu, Effects of Pt site distributions on the catalytic performance of Pt/SAPO-11 for n-dodecane hydroisomerization, Catal. Today 316 (2018) 43–50, https://doi.org/10.1016/j.cattod.2018.04.072.

[22] J. Zecevic, G. Vanbutsele, K.P. De Jong, J.A. Martens, Nanoscale intimacy in bifunctional catalysts for selective conversion of hydrocarbons, Nature 528 (2015) 245–254, https://doi.org/10.1038/nature16173.

[23] Y. Zhang, D. Liu, Z. Men, K. Huang, Y. Lv, M. Li, B. Lou, Hydroisomerization of n-dodecane over bi-porous Pt-containing bifunctional catalysts: effects of alkene intermediates' journey distances within the zeolite micropores, Fuel 236 (2019) 428–436, https://doi.org/10.1016/j.fuel.2018.09.017.

[24] M.G. Falco, S.A. Canavese, R.A. Comelli, N.S. Fígoli, Influence of Pt concentration on tungsten oxide-promoted zirconia during n-hexane isomerization, Appl. Catal. Gen. 201 (2000) 37–43, https://doi.org/10.1016/S0926-860X(00)00417-8.

[25] J.E. Samad, J. Blanchard, C. Sayag, C. Louis, J.R. Regalbuto, The controlled synthesis of metal-acid bifunctional catalysts: selective Pt deposition and nanoparticle synthesis on amorphous aluminosilicates, J. Catal. 342 (2016) 213–225, https://doi.org/10.1016/j.jcat.2016.08.002.

[26] D. Karthikeyan, R. Atchudan, R. Sivakumar, Effect of metal content on the activity and product selectivity of n-decane hydroisomerization over Ni-Pd/HY zeolite, Cuihua Xuebao/Chin. J. Catal. 37 (2016) 1907–1917, https://doi.org/10.1016/S1872-2067(16)62507-X.

[27] J. Dawody, M. Skoglundh, S. Wall, E. Fridell, Role of Pt-precursor on the performance of Pt/BaCO 3/Al 2O 3·NO x storage catalysts, J. Mol. Catal. Chem. 225 (2005) 259–269, https://doi.org/10.1016/j.molcata.2004.09.011.

[28] K. Chi, Z. Zhao, Z. Tian, S. Hu, L. Yan, T. Li, B. Wang, X. Meng, S. Gao, M. Tan, Y. Liu, Hydroisomerization performance of platinum supported on ZSM-22/ZSM-23 intergrowth zeolite catalyst, Petrol. Sci. 10 (2013) 242–250, https://doi.org/10.1007/s12182-013-0273-6.

[29] N. Chen, S. Gong, H. Shirai, T. Watanabe, E.W. Qian, Effects of Si/Al ratio and Pt loading on Pt/SAPO-11 catalysts in hydroconversion of Jatropha oil, Appl. Catal. Gen. 466 (2013) 105–115, https://doi.org/10.1016/j.apcata.2013.06.034.

[30] S.A. Karakoulia, E. Heracleous, A.A. Lappas, Mild hydroisomerization of heavy naphtha on mono- and bi-metallic Pt and Ni catalysts supported on Beta zeolite, Catal. Today (2019), https://doi.org/10.1016/j.cattod.2019.04.072.

[31] E.A. Paukshtis, A.S. Belyi, E.A. Belopukhov, V.A. Shkurenok, M.D. Smolikov, Investigation of the Pt/MOR–Al2O3 catalysts by IR spectroscopy, Procedia Eng. (2015) 19–25, https://doi.org/10.1016/j.proeng.2015.07.281.

[32] Z. Vít, D. Gulková, L. Kaluža, M. Boaro, Effect of catalyst precursor and its pretreatment on the amount of β-Pd hydride phase and HDS activity of Pd-Pt/silica-alumina, Appl. Catal. B Environ. 146 (2014) 213–220, https://doi.org/10.1016/j.apcatb.2013.02.055.

[33] E.R. Naranov, A.L. Maximov, Selective conversion of aromatics into cis-isomers of naphthenes using Ru catalysts based on the supports of different nature, Catal. Today 329 (2019) 94–101, https://doi.org/10.1016/j.cattod.2018.10.068.

[34] P. Mäki-Arvela, T. Kaka khel, M. Azkaar, S. Engblom, D. Murzin, Catalytic hydroisomerization of long-chain hydrocarbons for the production of fuels, Catalysts 8 (2018) 534, https://doi.org/10.3390/catal8110534.

[35] B.D. Chandler, A.B. Schabel, C.F. Blanford, L.H. Pignolet, Preparation and characterization of supported bimetallic Pt-Au particle catalysts from molecular cluster and chloride salt precursors, J. Catal. 187 (1999) 367–384, https://doi.org/10.1006/jcat.1999.2641.

[36] R.M. Antoniassi, L. Otubo, J.M. Vaz, A. Oliveira Neto, E.V. Spinacé, Synthesis of Pt nanoparticles with preferential (1 0 0) orientation directly on the carbon support for Direct Ethanol Fuel Cell, J. Catal. 342 (2016) 67–74, https://doi.org/10.1016/j.jcat.2016.07.022.

[37] L. Hu, K.A. Boateng, J.M. Hill, Sol-gel synthesis of Pt/Al2O3 catalysts: effect of Pt precursor and calcination procedure on Pt dispersion, J. Mol. Catal. Chem. 259 (2006) 51–60, https://doi.org/10.1016/j.molcata.2006.06.018.

[38] T. Lopez, P. Bosch, M. Moran, R. Gomez, Pt/SiO2 sol-gel catalysts: effects of pH and platinum precursor, J. Phys. Chem. 97 (1993) 1671–1677, https://doi.org/10.1021/j100110a033.

[39] L. Geng, J. Gong, G. Qiao, S. Ye, J. Zheng, N. Zhang, B. Chen, Effect of metal precursors on the performance of Pt/SAPO-11 catalysts for n -dodecane hydroisomerization, ACS Omega 4 (2019) 12598–12605, https://doi.org/10.1021/acsomega.9b01216.

[40] G. Pölczmann, J. Valyon, Á. Szegedi, R.M. Mihályi, J. Hancsók, Hydroisomerization of fischer-tropsch wax on Pt/AlSBA-15 and Pt/SAPO-11 catalysts, in: Top. Catal., 2011, pp. 1079–1083, https://doi.org/10.1007/s11244-011-9728-4.
[41] N. Batalha, L. Pinard, C. Bouchy, E. Guillon, M. Guisnet, N-Hexadecane hydroisomerization over Pt-HBEA catalysts. Quantification and effect of the intimacy between metal and protonic sites, J. Catal. 307 (2013) 122–131, https://doi.org/10.1016/j.jcat.2013.07.014.
[42] N. Batalha, S. Morisset, L. Pinard, I. Maupin, J.L. Lemberton, F. Lemos, Y. Pouilloux, BEA zeolite nanocrystals dispersed over alumina for n-hexadecane hydroisomerization, in: Microporous Mesoporous Mater., 2013, pp. 161–166, https://doi.org/10.1016/j.micromeso.2012.04.041.
[43] C.E. Hunt, Hydrogen chemisorption on platinum catalysts, J. Catal. 23 (1971) 93–96, https://doi.org/10.1016/0021-9517(71)90028-5.
[44] F. Regali, V. Montes, L.F. Liotta, S. Järås, A.M. Venezia, M. Boutonnet, Effect of metal loading on activity, selectivity and deactivation behavior of Pd/silica–alumina catalysts in the hydroconversion of n-hexadecane, in: Catal. Today, 2013, pp. 87–96, https://doi.org/10.1016/j.cattod.2013.08.028.
[45] X. Hao, L. Quach, J. Korah, W.A. Spieker, J.R. Regalbuto, The control of platinum impregnation by PZC alteration of oxides and carbon, J. Mol. Catal. Chem. 219 (2004) 97–107, https://doi.org/10.1016/j.molcata.2004.04.026.
[46] W.A. Spieker, J.R. Regalbuto, A fundamental model of platinum impregnation onto alumina, Chem. Eng. Sci. 56 (2001) 3491–3504, https://doi.org/10.1016/S0009-2509(01)00052-5.
[47] W. Spieker, J. Regalbuto, D. Rende, M. Bricker, Q. Chen, Experimental investigation and modeling of platinum adsorption onto ion-modified silica and alumina. https://doi.org/10.1016/s0167-2991(00)80957-x, 2007, 203-208.
[48] L. Jiao, J.R. Regalbuto, The synthesis of highly dispersed noble and base metals on silica via strong electrostatic adsorption: II. Mesoporous silica SBA-15, J. Catal. 260 (2008) 342–350, https://doi.org/10.1016/j.jcat.2008.09.023.
[49] P. Tavolaro, A. Tavolaro, G. Martino, Influence of zeolite PZC and pH on the immobilization of cytochrome c: a preliminary study regarding the preparation of new biomaterials, Colloids Surf. B Biointerfaces 70 (2009) 98–107, https://doi.org/10.1016/j.colsurfb.2008.12.019.
[50] Y. Kanda, T. Aizawa, T. Kobayashi, Y. Uemichi, S. Namba, M. Sugioka, Preparation of highly active AlSBA-15-supported platinum catalyst for thiophene hydrodesulfurization, Appl. Catal. B Environ. 77 (2007) 117–124, https://doi.org/10.1016/j.apcatb.2007.07.012.
[51] K. Jaroszewska, A. Masalska, J.R. Grzechowiak, J. Grams, Hydroconversion of 1-methylnaphthalene over Pt/AlSBA-15-Al2O3 composite catalysts, Appl. Catal. Gen. 505 (2015) 116–130, https://doi.org/10.1016/j.apcata.2015.07.021.
[52] L.D. Sharma, M. Kumar, A.K. Saxena, M. Chand, J.K. Gupta, Influence of pore size distribution on Pt dispersion in Pt-Sn/Al2O3 reforming catalyst, J. Mol. Catal. Chem. 185 (2002) 135–141, https://doi.org/10.1016/S1381-1169(01)00438-1.
[53] M. Subsadsana, P. Sangdara, C. Ruangviriyachai, Effect of bimetallic NiW modified crystalline ZSM-5 zeolite on catalytic conversion of crude palm oil and identification of biofuel products, Asia-Pacific, J. Chem. Eng. 12 (2017) 147–158, https://doi.org/10.1002/apj.2061.
[54] F. Güleç, F. Sher, A. Karaduman, Catalytic performance of Cu- and Zr-modified beta zeolite catalysts in the methylation of 2-methylnaphthalene, Petrol. Sci. 16 (2019) 161–172, https://doi.org/10.1007/s12182-018-0278-2.
[55] R. Thakur, S. Barman, R. Kumar Gupta, Synthesis of cumene by transalkylation over modified beta zeolite: a kinetic study, Braz. J. Chem. Eng. 33 (2016) 957–967, https://doi.org/10.1590/0104-6632.20160334s20150333.
[56] L. Jin, Y. Fang, H. Hu, Selective synthesis of 2,6-dimethylnaphthalene by methylation of 2-methylnaphthalene with methanol on Zr/(Al)ZSM-5, Catal, Commun. Now. 7 (2006) 255–259, https://doi.org/10.1016/j.catcom.2005.11.012.
[57] Y. Qiu, X. Hou, G. Liu, L. Wang, X. Zhang, Fast recovery of BrØnsted acid sites lost during high-temperature calcination in HZSM-5, Microporous Mesoporous Mater. 243 (2017) 176–185, https://doi.org/10.1016/j.micromeso.2017.02.030.
[58] K. Fang, J. Ren, Y. Sun, Effect of nickel precursors on the performance of Ni/AlMCM-41 catalysts for n-dodecane hydroconversion, J. Mol. Catal. Chem. 229 (2005) 51–58, https://doi.org/10.1016/j.molcata.2004.10.055.
[59] Y. Lyu, Z. Yu, Y. Yang, X. Wang, X. Zhao, X. Liu, Z. Yan, Metal-acid balance in the in-situ solid synthesized Ni/SAPO-11 catalyst for n-hexane hydroisomerization, Fuel 243 (2019) 398–405, https://doi.org/10.1016/j.fuel.2019.01.013.
[60] V. Akhmedov, S. Al-Khowaiter, Recent advances and future aspects in the selective isomerization of high n-alkanes, Catal. Rev. Sci. Eng. 49 (2007) 33–139, https://doi.org/10.1080/01614940601128427.